Applicability of the polynomial chaos expansion method for personalization of a cardiovascular pulse wave propagation model

INTERNATIONAL JOURNAL FOR NUMERICAL METHODS IN BIOMEDICAL ENGINEERING
Int. J. Numer. Meth. Biomed. Engng. 2014; **30**:1679–1704
Published online in Wiley Online Library (wileyonlinelibrary.com). DOI: 10.1002/cnm.2695

Applicability of the polynomial chaos expansion method for personalization of a cardiovascular pulse wave propagation model

W. Huberts[1,3,*,†,‡], W. P. Donders[2,*,†,‡], T. Delhaas[1] and F. N. van de Vosse[3]

[1]*Department of Biomedical Engineering, School of Cardiovascular Diseases (CARIM), Faculty of Health, Medicine and Life Sciences, Maastricht University*
[2]*Department of Biomedical Engineering, School of Mental Health and Neuroscience (MHENS), Faculty of Health, Medicine and Life Sciences, Maastricht University*
[3]*Department of Biomedical Engineering, Eindhoven University of Technology*

SUMMARY

Patient-specific modeling requires model personalization, which can be achieved in an efficient manner by parameter fixing and parameter prioritization. An efficient variance-based method is using generalized polynomial chaos expansion (gPCE), but it has not been applied in the context of model personalization, nor has it ever been compared with standard variance-based methods for models with many parameters. In this work, we apply the gPCE method to a previously reported pulse wave propagation model and compare the conclusions for model personalization with that of a reference analysis performed with Saltelli's efficient Monte Carlo method. We furthermore differentiate two approaches for obtaining the expansion coefficients: one based on spectral projection (gPCE-P) and one based on least squares regression (gPCE-R). It was found that in general the gPCE yields similar conclusions as the reference analysis but at much lower cost, as long as the polynomial metamodel does not contain unnecessary high order terms. Furthermore, the gPCE-R approach generally yielded better results than gPCE-P. The weak performance of the gPCE-P can be attributed to the assessment of the expansion coefficients using the Smolyak algorithm, which might be hampered by the high number of model parameters and/or by possible non-smoothness in the output space.

Received 21 May 2014; Revised 11 September 2014; Accepted 29 October 2014

KEY WORDS: sensitivity analysis; model personalization; patient-specific modeling; polynomial chaos expansion; uncertainty quantification

1. INTRODUCTION

In cardiovascular research, computational modeling has extensively been used for different purposes. Computational models have given insights into physiological [1–5] and pathophysiological phenomena [6–9] and have had a significant contribution to the design and evaluation of medical devices [10–13]. In addition, they have been used to develop training simulators for medical interventions [14–16] and to determine hemodynamic parameters that were not directly measurable [17–19]. In the past decade, these models have even become so mature that researchers have started aiming for the application of these models to enhance clinical diagnosis [20, 21] and/or to support clinical decision-making during surgical planning by patient-specifically predicting the outcome of an intervention [22, 23].

However, the translation of mathematical models to the clinic, either for diagnosis or for supporting clinical decision-making, is a challenge. One of the major difficulties is assessing patient-specific

*Correspondence to: Wouter Huberts, School of Cardioascular Diseases (CARIM), department of Biomedical Engineering, Faculty of Health, Medicine and Life Sciences, Maastricht University. PO Box 616, 6200 MD, Maastricht.
†E-mail: wouter.huberts@maastrichtuniversity.nl
‡Authors contributed equally.

boundary and initial conditions as well as numerical values of the model parameters (i.e. model personalization). It is impossible to determine all model parameters patient-specifically because measurement modalities are not available for all model parameters and, moreover, because the burden on the patient should be minimized. In addition, the precision and accuracy of clinical measurements are hampered by large biological and day-to-day variations, and by measurement uncertainties. The resulting sparse and uncertain datasets will result in uncertainty in model predictions, which will increase even further when the complexity of the model (i.e. the number of model parameters) is made larger. A simplification of the model may on the other hand significantly increase the uncertainty in the prediction because the model can no longer capture the relevant physics and physiology. Therefore, a balance is needed between the uncertainty resulting from model input parameters and the uncertainty resulting from model assumptions (Figure 1). For this, it is essential to quantify the uncertainty in the output resulting from model input and to determine whether the complexity of the model is sufficient for the application of interest. The output uncertainty resulting from model input can be quantified by performing an uncertainty analysis. To be sure that the output uncertainty is as low as possible, it is important that the measurement protocol is designed such that the model parameters affecting the output the most are measured with the highest accuracy. A sensitivity analysis can be used for protocol design as it is able to determine which model parameters are most rewarding to measure more accurately (parameter prioritization) and which model parameters can be fixed based on population-averaged data from literature or databases (parameter fixing) [26]. A proper sensitivity analysis in the setting of parameter prioritization and fixing is therefore indispensable for model personalization in predictive modeling.

Variance-based global sensitivity analysis methods are currently considered to be the best practice with respect to parameter prioritization and fixing [26–28]. As opposed to many other sensitivity analysis methods, they are applicable to any model, regardless the model's properties with respect to linearity, monotonicity, and/or additivity (a nonadditive model has interactions between model parameters). Moreover, the method is able to apportion each fraction of the output uncertainty (variance) to the direct effects of single input parameters (main sensitivity indices) or to the combined effects of multiple (k) model parameters (higher-order sensitivity indices) for a total of $2^k - 1$ sensitivity indices. To reduce computational cost, the higher-order effects are mostly considered by using the total sensitivity index introduced by Homma *et al.* [29], which is the sum of the main sensitivity index of a parameter and all the higher-order sensitivity indices in which this parameter is involved. The main sensitivity indices are useful for parameter prioritization, whereas the total sensitivity indices are used for parameter fixing [26, 27].

Several numerical approaches are available to estimate these variance-based sensitivity indices. These approaches require multiple model runs in a Monte Carlo simulation. The most straightforward method is the crude Monte Carlo method, which requires $\mathcal{O}(k \cdot 10^6)$ model runs, where k is the number of model parameters [26]. Saltelli *et al.* [30] introduced a method to estimate the indices using only $\mathcal{O}(k \cdot 10^3)$ model runs. For details on the computational costs of these methods, see Appendix B.

However, large computing resources are still required for models with many parameters, even when Saltelli's method is applied. An alternative method is to construct a metamodel and to calculate the sensitivity indices of the metamodel. The (generalized) polynomial chaos expansion (gPCE)

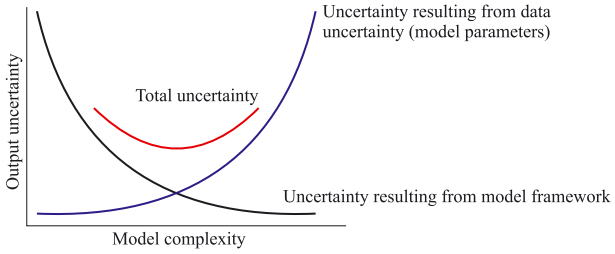

Figure 1. The contents of the uncertainty of prediction with personalized models are shown as functions of model complexity. Adapted from the work in [24, 25].

DOI: 10.1002/cnm

method creates a metamodel by spanning the model output space with orthogonal polynomial basis functions that are dependent on the stochastic model input parameters [31–34]. The gPCE is an attractive metamodeling method for global variance-based sensitivity analysis because once the expansion coefficients are known it can be easily decomposed to find the sensitivity indices [32, 33].

To find the expansion coefficients, a spectral projection or regression approach can be used. The spectral projection approach determines the coefficients by projecting the output on the normalized basis functions by using inner products and exploiting the orthogonality of the basis functions. This projection requires integration over the input domain, which can be carried out efficiently by constructing a sparse grid on the input space using the Smolyak algorithm [35–38] and running the model for each sparse grid point. This approach can exhibit spectral convergence when the output depends smoothly on the input parameters [31, 32, 34]. Conversely, the regression method does not require integration and determines the expansion coefficients by finding a least square fit of the gPCE on the points in the output space. As a consequence, the regression approach is not dependent on the accuracy of any particular integration scheme.

The gPCE method using spectral projection and sparse grid integration can be much more efficient than the Monte Carlo method of Saltelli ($\mathcal{O}\left(\frac{2^l k^l}{l!}\right)$ model runs, with l as the sparse grid level) [31, 34]. This is also true for the regression approach when the same sparse grid samples are used. An additional advantage of the gPCE is that it automatically yields all $2^k - 1$ sensitivity indices. Moreover, it provides insight into the dependencies of the output with respect to the input parameters (e.g. squared and third power) without the need to create scatter plots. These advantages advocate for the use of gPCE for model personalization. However, a major drawback of the gPCE is that the number of basis functions grows exponentially when the number of model parameters increases [32]. These functions need to be evaluated in the sample points, which can become a significant portion of the total computational cost. Moreover, the number of expansion functions also reflects the number of expansion coefficients to be calculated, and thus, the sparse grid level l may need to increase to accommodate this.

The identification of important model parameters and the quantification of model output uncertainties resulting from model input uncertainties are still in its infancy in the field of cardiovascular modeling, as evidenced by the limited available literature on this topic with respect to the extensive number of cardiovascular model applications. Consequently, the optimal approach for model personalization has not been found yet. Nevertheless, some studies did apply a global sensitivity and uncertainty analysis on cardiovascular models. Wenk *et al.* [39] applied the method of Saltelli to examine the effects of atherosclerotic plaque parameters on the maximum circumferential stress. However, they only considered three model parameters (i.e. cap thickness, position of the region of microcalcifications, and its volume fraction).

Xiu *et al.* [40] successfully applied gPCE on a one-dimensional pulse wave propagation model to assess the output velocity uncertainty resulting from the stiffness input parameters of the vessels included ($k = 37$ in total). However, they performed uncertainty analysis using gPCE but did not use gPCE in the context of parameter fixing and parameter prioritization. We have developed a pulse wave propagation model to support vascular access surgery planning [22] (Figure 2). This model was used for patient-specific selection of the optimal location for vascular access creation that is essential for hemodialysis treatment [41]. To personalize the model, we applied the variance-based sensitivity analysis for $k = 73$ parameters using the Saltelli method to assess the important model parameters with respect to parameter prioritization and fixing [42, 43].

To our knowledge, the gPCE method has not yet been used in the setting of parameter prioritization and fixing (i.e. to personalize a predictive model). Moreover, in case of many model parameters ($k > 50$), it was also not yet determined whether the gPCE method yields similar conclusions as the Saltelli method. Therefore, the aim of this study is to apply the gPCE method to our previously developed pulse wave propagation model and to examine whether this method results in the same conclusions with respect to model personalization (parameter fixing and prioritization) as the Saltelli method. In addition, we will investigate the influence of using the spectral projection or regression approach for assessing the gPCE coefficients. We selected this pulse wave propagation model because it has a high number of model parameters ($k = 73$) and because it already proved its potential in clinical decision-making [22].

DOI: 10.1002/cnm

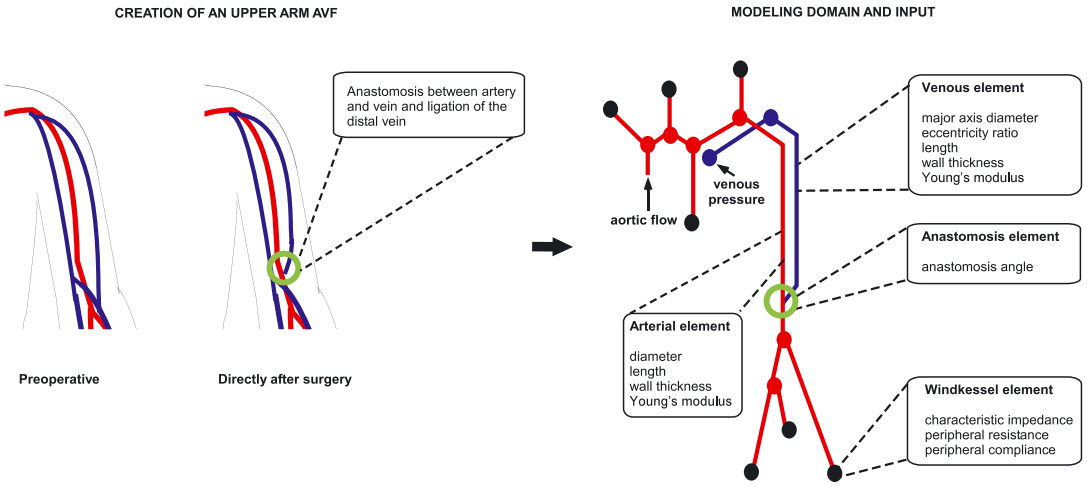

Figure 2. A brief overview of the model to which the sensitivity analysis is applied. Uncertain input parameters are described for each model element.

The article is outlined as follows. First, we will describe the mathematical basis of variance-based global sensitivity analysis and introduce the main and total sensitivity indices. It will be described how these indices can be used for model personalization. Second, we will describe the gPCE and how it can be used to derive the main and total sensitivity indices. Then we will describe the projection and the expansion approaches for finding the expansion coefficients. Third, we introduce the pulse wave propagation model to which the sensitivity analysis will be applied and explain how we will compare the conclusions for model personalization derived from gPCE to the conclusions derived from a reference analysis. Finally, the results of the gPCE method are compared with that of the Saltelli method and discussed, with particular emphasis on their conclusions with respect to parameter prioritization and fixing (model personalization).

2. VARIANCE-BASED SENSITIVITY ANALYSIS

In this section, we will explain the variance-based sensitivity analysis and how it can be used for model personalization. For formal notations and details, we refer to the available mathematical literature; for example, [26, 27, 44].

2.1. Variance-based sensitivity analysis

2.1.1. Mathematical description. Consider a model $Y=f(X_1,\ldots,X_k)$ as a function of its stochastic model input parameters X_i, $i=1,\ldots,k$, which are defined on the domain $\Omega=\Omega_1\times\Omega_2\times\cdots\times\Omega_k$ with $\{\Omega_i=[0,1]\}$. Sobol decomposed $f(X_1,\ldots,X_k)$ into summands with increasing dimensionality; that is,

$$f(X_1,\ldots,X_k)=f_0+\sum_{i_1=1}^{k}f_{i_1}\left(X_{i_1}\right)+\sum_{i_1=1}^{k}\sum_{i_2>i_1}^{k}f_{i_1,i_2}\left(X_{i_1},X_{i_2}\right)+\ldots+f_{12\ldots k}(X_1,\ldots,X_k), \quad (1)$$

where $f_0=\mathrm{E}(Y)$ is the expected value of Y and each summand has zero mean and the following property to ensure orthogonality:

$$\int_{\Omega_k}f_{i_1,\ldots,i_s}(X_{i_1},\ldots,X_{i_s})\mathrm{d}x_k=0 \quad \text{for} \quad k=i_1,\ldots,i_s, \quad (2)$$

with $1\leqslant i_1<\cdots<i_s\leqslant k$ and $s=1,\ldots,k$ [44] (see also Appendix A). Assuming a uniform

DOI: 10.1002/cnm

probability density function on the domain Ω, the total variance $\mathrm{V}(Y)$ of the model is given by

$$\mathrm{V}(Y) = \int_{\Omega} (f(X_1, \ldots, X_k) - \mathrm{E}(Y))^2 \mathrm{d}\Omega = \int_{\Omega} (f(X_1, \ldots, X_k) - f_0)^2 \mathrm{d}\Omega. \tag{3}$$

The total variance of Y can be written by taking the variance of each summand in Equation (1) and using the property in Equation (2) as follows:

$$\mathrm{V}(Y) = \sum_{i_1=1}^{k} V_{i_1} + \sum_{i_1=1}^{k} \sum_{i_2>i_1}^{k} V_{i_1,i_2} + \ldots + V_{12\ldots k}, \tag{4}$$

with V_{i_1}, V_{i_1,i_2}, and $V_{12\ldots k}$ partial variances defined as

$$V_{i_1,\ldots,i_s} = \int_{\Omega_{i_1}} \ldots \int_{\Omega_{i_s}} f^2_{i_1,\ldots,i_s}(X_{i_1}, \ldots, X_{i_s}) \mathrm{d}\Omega_{i_1} \ldots \mathrm{d}\Omega_{i_s}. \tag{5}$$

By normalizing with the total variance $\mathrm{V}(Y)$, the variance decomposition in Equation (4) becomes

$$1 = \sum_{i=1}^{k} S_{i_1} + \sum_{i_1=1}^{k} \sum_{i_2>i_1}^{k} S_{i_1,i_2} + \ldots + S_{12\ldots k}, \tag{6}$$

in which S_{i_1} are the main sensitivity indices, whereas the second (S_{i_1,i_2}) and higher ($S_{i_1,i_2,\ldots,i_s}$) order sensitivity indices are measures for the interaction effects of the involved parameters on the total output variance.

2.1.2. *Interpretation for model personalization.*

2.1.2.1. Parameter prioritization. The main sensitivity index $S_{i_1} = V_{i_1}/\mathrm{V}(Y) = \mathrm{V}(\mathrm{E}(Y|X_{i_1}))/\mathrm{V}(Y)$ (with $i_1 = 1, \ldots, k$) is very useful for parameter prioritization as this index represents the expected reduction in variance if the true values of model parameter X_{i_1} were known exactly without uncertainty. The main sensitivity indices can assist in rationally choosing (under uncertainty) which parameters should be determined as accurately as possible to obtain the largest reduction in variance.

2.1.2.2. Parameter fixing. To determine which model parameters can be fixed, interactions between the model parameters need to be considered because the first-order effect of a parameter can be very low, whereas its contribution in the interaction with other terms can be very large. In other words, the higher-order sensitivity indices need to be considered for parameter fixing. Homma *et al.* [29] introduced the total sensitivity index that is defined as the sum of all the sensitivity indices in Equation (6) in which the model parameter of interest is involved. Suppose now that we fix all model parameters on their true value except model parameter X_{i_1} (with $i_1 = 1, \ldots, k$). The only sensitivity terms that will be left unexplained in Equation (6) are the terms in which model parameter X_{i_1} is involved. When considering the properties of the partial variances in Equation (5), it can be shown that all sensitivity terms in which model parameter X_{i_1} is not involved is captured by $S_{-i_1} = \mathrm{V}(\mathrm{E}(Y|\boldsymbol{X}_{-i_1}))/\mathrm{V}(Y)$ in which the subscript $-i_1$ means all model parameters except model parameter X_{i_1}. Consequently, the total sensitivity index S_{T,i_1} that captures all terms in which X_{i_1} is involved can be written as $S_{\mathrm{T},i_1} = 1 - \mathrm{V}\left(\mathrm{E}\left(Y|\boldsymbol{X}_{-i_1}\right)\right)/\mathrm{V}(Y) = \mathrm{E}\left(\mathrm{V}\left(Y|\boldsymbol{X}_{-i_1}\right)\right)/\mathrm{V}(Y)$ [26, 30]. Thus, the total sensitivity index is by definition the expected residual variance if all parameters except X_{i_1} are known and fixed on their true value. If this residual variance is low (low total sensitivity index), the parameter is non-influential. Therefore, the total sensitivity index can be used to determine which parameter is non-influential and can, as a result, be fixed within its uncertainty range.

DOI: 10.1002/cnm

3. GENERALIZED POLYNOMIAL CHAOS EXPANSION

In this section, the formulation of the gPCE will be given. Thereafter, it will be explained how a polynomial chaos expansion with known coefficients can be used for model personalization by estimating the main and total sensitivity indices. Then two approaches for calculating the expansion coefficients are explained. First, the spectral projection approach and then the least squares regression approach will be presented. For more details, we refer to the literature [32–34].

3.1. Formulation of the polynomial chaos expansion

Following the theory of gPCE, any stochastic output parameter can be spanned by multivariate orthogonal polynomials that are functions of the independent stochastic input parameters. Different types of multivariate polynomials should be chosen based on the distribution of the stochastic parameters to achieve better convergence. For example, Hermite polynomials are preferred in case of Gaussian distributed input parameters as these polynomials are orthogonal with respect to the Gaussian measure, whereas Legendre polynomials are preferred in case of uniform distributions [32]. Moreover, it can be shown that such an expansion is convergent in the L_2-norm [32].

We consider a stochastic output $Y = f(X_1, X_2, \ldots, X_k)$ as a function of its uniformly distributed stochastic input parameters. As opposed to the previous section, the domain of each parameter X_i is $\Omega_i = [-1, +1]$ to accommodate the domain of the Legendre polynomials. The infinite polynomial chaos expansion can be truncated to include only polynomials up to a maximal polynomial order z:

$$Y = f(X_1, \ldots, X_k) \approx f_{\text{gPCE}}(X_1, \ldots, X_k) = \sum_{j=0}^{P-1} c_j \Psi_j(X_1, \ldots, X_k). \tag{7}$$

Here, $\Psi_j(X_1, \ldots, X_k)$ are the multivariate Legendre polynomials, and $P = \binom{z+k}{z}$ is the number of unknown expansion coefficients c_j. After introducing the integer sequence

$$\boldsymbol{\alpha} = \{\alpha_i, i = 1, \ldots, k\}, \quad \alpha_i \geqslant 0, \quad \sum_{i=1}^{k} \alpha_i \leqslant z, \tag{8}$$

each multivariate polynomial can be represented by its own integer sequence $\boldsymbol{\alpha}^j$ as follows:

$$\Psi_j \equiv \Psi_{\boldsymbol{\alpha}^j}(X_1, \ldots, X_k) = \prod_{i=1}^{k} \psi_{\alpha_i^j}(X_i), \tag{9}$$

in which $\psi_{\alpha_i^j}$ is the univariate Legendre polynomial of order α_i^j. Note that the zeroth-order Legendre polynomial $\psi_0 = 1$. To determine the integer sequences $\boldsymbol{\alpha}^j$ for $j = 0, \ldots, P-1$ for a given number of parameters k and maximal polynomial order z, we used the algorithm described in [45]. Equation (7) can also be stated as follows:

$$f_{\text{gPCE}} = \sum_{j=0}^{P-1} c_{\boldsymbol{\alpha}^j} \Psi_{\boldsymbol{\alpha}^j}(X_1, \ldots, X_k). \tag{10}$$

The formulations of Equations (7) and (10) will both be used in the remainder of this work based on ease of notation in each instance.

3.2. Sobol decomposition of the truncated polynomial chaos expansion

Consider that each multivariate Legendre polynomial $\Psi_{\boldsymbol{\alpha}^j}(X_1, \ldots, X_k)$ is the product of k univariate Legendre polynomials $\psi_{\alpha_i^j}(X_1)$, computed with Equation (9). The multivariate polynomial is constant (equal to 1) along each dimension i that is spanned by a zeroth-order univariate polynomial.

DOI: 10.1002/cnm

Therefore, the multivariate polynomial Ψ can be considered a function of the remaining parameters only. By slight abuse of notation, we introduce the set $\boldsymbol{A}_{i_1}^{i_s}$:

$$\boldsymbol{A}_{i_1}^{i_s} = \left\{\boldsymbol{\alpha} \,|\, \alpha_i > 0 \quad \forall i \in \{i_1, \ldots, i_s\}, \alpha_j = 0 \quad \forall j \notin \{i_1, \ldots, i_s\}\right\}, \tag{11}$$

which is the set of all integer sequences $\boldsymbol{\alpha}$ that have a positive component in the parameter dimension i, with $1 \leqslant i_1 \leqslant i \leqslant i_s \leqslant k$, and zero elsewhere. Now it is straightforward to decompose the truncated polynomial chaos expansion into summands of increasing dimensionality:

$$\begin{aligned} f_{\mathrm{gPCE}} = f_0 &+ \sum_{i_1=1}^{k} \left(\sum_{\boldsymbol{\alpha} \in \boldsymbol{A}_{i_1}^{i_1}} c_{\boldsymbol{\alpha}} \Psi_{\boldsymbol{\alpha}}(X_{i_1}) \right) + \sum_{i_1=1}^{k} \sum_{i_2>i_1}^{k} \left(\sum_{\boldsymbol{\alpha} \in \boldsymbol{A}_{i_1}^{i_2}} c_{\boldsymbol{\alpha}} \Psi_{\boldsymbol{\alpha}}(X_{i_1}, X_{i_2}) \right) + \ldots \\ &+ \sum_{i_1=1}^{k} \sum_{i_2>i_1}^{k} \cdots \sum_{i_s>i_{s-1}}^{k} \left(\sum_{\boldsymbol{\alpha} \in \boldsymbol{A}_{i_1}^{i_s}} c_{\boldsymbol{\alpha}} \Psi_{\boldsymbol{\alpha}}(X_{i_1}, \ldots, X_{i_s}) \right) + \ldots \\ &+ \left(\sum_{\boldsymbol{\alpha} \in \boldsymbol{A}_{1}^{k}} c_{\boldsymbol{\alpha}} \Psi_{\boldsymbol{\alpha}}(X_1, \ldots, X_k) \right). \end{aligned} \tag{12}$$

Here, $f_0 = \mathrm{E}(f_{\mathrm{gPCE}})$ is the expected value of the truncated expansion f_{gPCE}. Equation (12) is unique [34] and can therefore be identified as the Sobol decomposition of the truncated polynomial chaos expansion (*cf.* Equation (1)). The Sobol summands are given by

$$f_{i_1,\ldots,i_s}(X_{i_1}, \ldots, X_{i_s}) = \sum_{\boldsymbol{\alpha} \in \boldsymbol{A}_{i_1}^{i_s}} c_{\boldsymbol{\alpha}} \Psi_{\boldsymbol{\alpha}}, \tag{13}$$

with $1 \leqslant i_1 < \cdots < i_s \leqslant k$ and $s = 1, \ldots, k$. The sensitivity indices $S_{i_1,\ldots,i_s}$ are retrieved after taking the variance of the summands and dividing by the total variance $\mathrm{V}(f_{\mathrm{gPCE}}) = \sum_{\boldsymbol{\alpha}} c_{\boldsymbol{\alpha}}^2 \mathrm{E}(\Psi_{\boldsymbol{\alpha}})^2$:

$$S_{i_1,\ldots,i_s} = \frac{1}{\mathrm{V}(f_{\mathrm{gPCE}})} \sum_{\boldsymbol{\alpha} \in \boldsymbol{A}_{i_1}^{i_s}} c_{\boldsymbol{\alpha}}^2 \mathrm{E}\left(\Psi_{\boldsymbol{\alpha}}^2\right). \tag{14}$$

The main sensitivity indices S_{i_1}, $i_1 = 1, \ldots, k$ are obtained from Equation (14) when $s = 1$. The total sensitivity indices S_{T,i_1} can be obtained by summing the fractional variances of all summands containing parameter i_1. We introduce the set $\boldsymbol{B}_{i_1}$:

$$\boldsymbol{B}_{i_1} = \{\boldsymbol{\alpha} \,|\, \alpha_i > 0 \quad \forall i = i_1\}, \tag{15}$$

which is the set of all integer sequences $\boldsymbol{\alpha}$ where component i_1 has a positive value. Now the total sensitivity indices S_{T,i_1} are given by

$$S_{\mathrm{T},i_1} = \sum_{\boldsymbol{\alpha} \in \boldsymbol{B}_{i_1}} c_{\boldsymbol{\alpha}}^2 \mathrm{E}\left(\Psi_{\boldsymbol{\alpha}}^2\right). \tag{16}$$

The expected values of the squared polynomial basis functions $\Psi_{\boldsymbol{\alpha}}$ are known analytically:

$$\mathrm{E}\left(\Psi_{\boldsymbol{\alpha}}^2\right) = \prod_{i=1}^{k} \mathrm{E}\left(\psi_{\alpha_i}^2(X_i)\right) = \frac{1}{2\alpha_i + 1}, \tag{17}$$

assuming a uniform probability density function over the domain $[-1, 1]$ [34]. Therefore, it is possible to calculate the sensitivity indices once the expansion coefficients $c_{\boldsymbol{\alpha}}$ are known.

DOI: 10.1002/cnm

3.3. Computation of the expansion coefficients

To find the main and total sensitivity indices, the expansion coefficients $c_{\boldsymbol{\alpha}}$ must be known. There are two commonly used approaches to find the coefficients: spectral projection with sparse grid integration or least squares regression.

3.3.1. Spectral projection approach. The spectral projection approach exploits the orthogonality of the basis functions. Because of this orthogonality, in analog to Fourier transformation, the expansion coefficients can be written as

$$c_{\boldsymbol{\alpha}} = \frac{\int_{\Omega} Y \Psi_{\boldsymbol{\alpha}} \rho \mathrm{d}\Omega}{\int_{\Omega} \Psi_{\boldsymbol{\alpha}}^2 \rho \mathrm{d}\Omega}, \qquad \forall \boldsymbol{\alpha}. \tag{18}$$

Herein, ρ is the joint probability density function that can be written as $\rho(X_1, \ldots, X_k) = \prod_{i=1}^{k} p_{r,i}(X_i)$ in case of independent model parameters. Note that the marginal distribution function $p_{r,i} = \frac{1}{2}$ for uniformly distributed and independent model parameters defined on the domain $[-1, 1]$. To determine the expansion coefficients, the integrals in Equation (18) need to be calculated. The denominator is the expected value of $\Psi_{\boldsymbol{\alpha}}$, which is known analytically. The numerator will be approximated by efficiently using tensor products of one-dimensional quadrature formulas by using the Smolyak algorithm [36]. In this work, we used Clenshaw–Curtis quadrature formulas that use the extrema of Chebyshev polynomials as nodal points. The nodal point sets are nested for different grid levels l, which significantly reduce the number of grid points. This method has been proved to give good results for smooth integrands in high ($k > 8$) dimensions by Novak and Ritter [35] and is described for its application in polynomial chaos expansion by Xiu *et al.* [32, 33]. Details can furthermore be found in Appendix C.

3.3.2. Regression approach. The regression approach minimizes the error between the polynomial chaos expansion and the actual model output in a least squares sense for a given set of expansion coefficients $\boldsymbol{C} = \{c_j, j = 0, \ldots, P-1\}$. Note that $c_j \equiv c_{\boldsymbol{\alpha}}$ and $\Psi_j \equiv \Psi_{\boldsymbol{\alpha}}$ as before. The approach attempts to find the set $\boldsymbol{C}$ that minimizes the sum of squared differences between the model output Y and the metamodel output f_{gPCE} (7):

$$\boldsymbol{C} = \operatorname{argmin} \frac{1}{N_{\mathrm{s}}} \sum_{i=1}^{N_{\mathrm{s}}} \left(Y(\boldsymbol{x}_i) - \sum_{j=0}^{P-1} c_j \Psi_j(\boldsymbol{x}_i) \right)^2, \tag{19}$$

where N_{s} is the number of input samples $\boldsymbol{x}_i$. By denoting the $N_{\mathrm{s}} \times P$ matrix $\underline{\Psi}$ where $\Psi_{ij} = \Psi_j(\boldsymbol{x}_i)$ the solution to Equation (19) is given by [34]

$$\underset{\sim}{C} = (\underline{\Psi}^T \underline{\Psi})^{-1} \underline{\Psi}^T \underset{\sim}{Y}, \tag{20}$$

where $\underset{\sim}{Y}$ is the column vector containing the model outputs for the input points $\boldsymbol{x}_i$, $i = 1, \ldots, N_{\mathrm{s}}$, and $\underset{\sim}{C}$ the column vector containing the expansion coefficients c_j, $j = 0, \ldots, P-1$. This is the (least squares) solution to the linear system $\underline{\Psi}\underset{\sim}{C} = \underset{\sim}{Y}$.

4. SIMULATIONS AND ANALYSIS

In this section, we will first introduce the model and its outputs of interest, which polynomial chaos expansion is applied. Thereafter, we will state which simulations we will perform and how we will compare the results from the polynomial chaos expansion with the results obtained from a reference analysis.

DOI: 10.1002/cnm

4.1. Pulse wave propagation model: reference

The pulse wave propagation model used in this study is extensively described by Huberts *et al.* [22], and therefore, only a brief description will be given here. The model simulates the postoperative flow after the creation of an arteriovenous fistula for hemodialysis. This arteriovenous fistula can be surgically created in two locations, and the model attempts to aid in this decision by simulating postoperative flows for both scenarios.

The model consists of serially connected lumped elements mimicking the local relation between pressure and flow (Figure 2). Three different types of elements were used: that is, vascular elements based on one-dimensional pulse wave propagation theory [5, 46], an anastomosis element based on semiempirical flow investigations in hydraulic T-junctions [47–49], and Windkessel elements to truncate the vascular geometry [50].

The model consists of 73 stochastic input parameters. The uncertainty domains of these parameters are presented in Table I. They are based on patient measurements and population spreads. For details, we refer to [42]. The outputs of interest are the mean brachial flow and the systolic pressure distal to the fistula (radial artery at wrist level). We previously performed a global variance-based sensitivity analysis using Saltelli's efficient Monte Carlo method for these outputs [42, 43]. However, for this work, we redo the same analysis but use a stricter convergence norm in the model as this slightly improves the results. Based on the previous study [43], we consider results obtained using $N = 5 \cdot 10^3$ runs per model parameter (resulting in $3.75 \cdot 10^5$ model runs) as a reference.

4.2. Sensitivity analysis using polynomial chaos expansion

Sensitivity analysis using gPCE will be carried out with expansions truncated at maximal polynomial orders $z \in \{1, 2, 3\}$ (corresponding to $P \in \{74, 2775, 70300\}$ polynomial basis functions with unknown coefficients) and sparse grid levels $l \in \{1, 2\}$ (corresponding to $N_s \in \{147, 10805\}$ sparse grid points). Both the spectral projection approach and the regression approach will be used to assess the expansion coefficients. As input samples for the regression approach, the sparse grid sample points constructed with the Smolyak algorithm are used to allow for the comparison of the two approaches.

Adjusted R^2-values are calculated for all combinations of metamodel order z and sparse grid level l for both gPCE approaches to quantify how well the metamodel f_{gPCE} is able to reconstruct the model output f. The adjusted R^2-values, $\bar{R}^2$, are calculated by

$$\bar{R}^2 = 1 - (1 - R^2)\frac{N_s - 1}{N_s - P - 1}, \tag{21}$$

with N_s the number of sparse grid points, P the number of unknown expansion coefficients, and R^2 defined by

$$R^2 = 1 - \frac{\sum_{i=1}^{N_s} (f(\boldsymbol{x}_i) - f_{\text{gPCE}}(\boldsymbol{x}_i))^2}{\sum_{i=1}^{N_s} (f(\boldsymbol{x}_i) - \overline{f})^2}. \tag{22}$$

4.2.1. Comparison to reference: parameter fixing. Parameters that have a low total sensitivity index can be fixed within their uncertainty range. A parameter X_i is considered fixable if its total sensitivity index is lower than a threshold value T:

$$X_i \begin{cases} \text{fixable}, & \text{if} \quad S_{T,i} < T = \frac{1}{k} \sum_{j=1}^{k} S_{T,j} \\ \text{non-fixable}, & \text{otherwise} \end{cases}. \tag{23}$$

The results for parameter fixing will be presented in a separate figure for each output of interest. Each figure will contain a tableau of plots for each chosen combination of metamodel (z) and approach for obtaining the expansion coefficients. Each plot will show the estimated total sensitivity

DOI: 10.1002/cnm

Table I. The input parameters and their uncertainty intervals.

No.	Parameter	Uncertainty interval [%]	No.	Parameter	Uncertainty interval (%)
	Arterial lengths			Arterial Young's moduli	
1	Innominate, subclavian, axillary, and brachial	$-10, 10$	36	Innominate, subclavian, axillary, brachial	$-20-20$
2	Radial	$-10, 10$	37	Radial	$-20-20$
3	Ulnar proximal and distal	$-10, 10$	38	Ulnar	$-20, 20$
4	Interosseus	$-10, 10$	39	Interosseus	$-20, 20$
5	Ascending aorta, aortic arch, thoracic aorta	$-10, 10$	40	Ascending aorta, aortic arch, thoracic aorta	$-20, 20$
	Venous lengths			Venous Young's moduli	
6	Median cubital and basilic veins [a]	$-10, 10$	41	Median cubital, basilic [a]	$-20, 20$
7	Cephalic, axillary, and subclavian [b]	$-10, 10$	42	Cephalic, axillary, subclavian [b]	$-20, 20$
	Arterial diameter tapering			Characteristic impedances	
8	Innominate, subclavian, axillary, and brachial	$-10, 10$	43	Right carotid artery	$-20, 20$
9	Radial	$-10, 10$	44	Left subclavian artery	$-20, 20$
10	Ulnar proximal and distal	$-10, 10$	45	Radial artery	$-20, 20$
11	Interosseus	$-10, 10$	46	Distal ulnar artery	$-20, 20$
12	Ascending aorta, aortic arch, thoracic aorta	$-10, 10$	47	Interosseus artery	$-20, 20$
	Venous diameter tapering		48	Vertebral artery	$-20, 20$
13	Median cubital and basilic [a]	$-10, 10$	49	Thoracic aorta	$-20, 20$
14	Cephalic, axillary, and subclavian [b]	$-10, 10$	50	Left carotid artery	$-20, 20$
	Arterial diameters			Windkessel resistances	
15	Innominate, subclavian, axillary, and brachial	$-10, 10$	51	Right carotid artery	$-25, 25$
16	Radial	$-10, 10$	52	Left subclavian artery	$-25, 25$
17	Ulnar proximal and distal	$-10, 10$	53	Radial artery	$-25, 25$
18	Interosseus	$-10, 10$	54	Distal ulnar artery	$-25, 25$
19	Ascending aorta, aortic arch, thoracic aorta	$-10, 10$	55	Interosseus artery	$-25, 25$
	Venous diameters		56	Vertebral artery	$-25, 25$
20	Median cubital and basilic [a]	$-10, 10$	57	Thoracic aorta	$-25, 25$
21	Cephalic, axillary, and subclavian [b]	$-10, 10$	58	Left carotid artery	$-25, 25$
	Change in arterial wall thickness			Windkessel compliances	
22	Innominate, subclavian, axillary, and brachial	$-40, 40$	59	Right carotid artery	$-50, 50$
23	Radial	$-40, 40$	60	Left subclavian artery	$-50, 50$
24	Ulnar proximal and distal	$-40, 40$	61	Radial artery	$-50, 50$
25	Interosseus	$-40, 40$	62	Distal ulnar artery	$-50, 50$
26	Ascending aorta, aortic arch, thoracic aorta	$-40, 40$	63	Interosseus artery	$-50, 50$
	Change in venous wall thickness		64	Vertebral artery	$-50, 50$
27	Median cubital, basilic [a]	$-40, 40$	65	Thoracic aorta	$-50, 50$
28	Cephalic, axillary, and subclavian [b]	$-40, 40$	66	Left carotid artery	$-50, 50$
	Arterial wall thickness			Other	
29	Subclavian, axillary, and brachial	$-40, 40$	67	Intravenous pressure	$-50, 50$
30	Radial artery	$-40, 40$	68	Eccentricity ratio of median cubital and basilic veins [a]	1.3,1.9[c]
31	Ulnar proximal and distal	$-40, 40$	69	Eccentricity ratio of cephalic, axillary, and subclavian veins [b]	1.3,1.9[c]
32	Interosseus	$-40, 40$	70	Anastomosis angle	15,90 [c]
33	Ascending aorta, aortic arch, thoracic aorta	$-40, 40$	71	Distributed flow	$-40, 40$
	Venous wall thickness		72	Mean brachial pressure	$-10, 10$
34	Median cubital, basilic [a]	$-40, 40$	73	Mean aortic flow	$-10, 10$
35	Cephalic, axillary, and subclavian [b]	$-40, 40$			

Edges that are changed simultaneously are separated by commas. Note that for the upper arm arteriovenous fistula (AVF) some venous edges are not in the model and therefore the related parameters are by definition non-influential in the upper arm AVF configuration.
[a]For an upper arm AVF, the basilic, axillary, and subclavian veins are combined.
[b]Not used in the model for an upper arm AVF.
[c]The absolute value [−] is presented.

DOI: 10.1002/cnm

index against the reference total sensitivity index of all parameters that are identified by gPCE as important (i.e. the parameters that will not be fixed). Horizontal and vertical dotted lines will indicate the threshold value T, and a diagonal dotted line will represent the agreement line. The number of parameters that are considered important by the gPCE method but not by the reference analysis is given by ϵ_{i}, and the number of parameters that are fixable according to the gPCE method but not fixable according to the reference is given by ϵ_{f}.

4.2.2. Comparison to reference analysis: parameter prioritization. Prioritization of parameters is obtained by ranking the important parameters based on their main sensitivity index. The rank of each important parameter in the reference set of important parameters is estimated by ranking the parameters based on the main sensitivity indices obtained using the gPCE method.

The results for parameter prioritization will be presented in a separate figure for each output of interest. Each figure will contain a tableau of plots for each chosen combination of metamodel z and the approach used for obtaining the expansion coefficients. Each plot will show the estimated rank of each parameter with an estimated total sensitivity index higher than the threshold T against the rank of that parameter according to the reference. For parameter prioritization, it is required that the set of important (non-fixable) parameters is identified correctly during parameter fixing. In addition, accurate values for the main sensitivity indices of the important parameters are required because we aim for a priority ranking based on the largest reduction in the output variance that is expected by accurately measuring that parameter.

5. RESULTS

To check our implementation of the polynomial chaos expansion, we investigated the convergence behavior of the gPCE results for several analytical functions with known sensitivity values (Appendix D). We found comparable behavior as reported in the literature (data not shown). We will denote the results obtained with the projection approach as gPCE-P and the results obtained with the regression approach as gPCE-R.

5.1. Pulse wave propagation model: reference

The results of the reference analysis using Saltelli's method with $N = 5 \cdot 10^3$ runs per model parameter are shown for both outputs of interest in Tables II and III for the main and total sensitivity indices, respectively.

Table II. Rounded reference values (%) corresponding to the main Sobol index of important parameters (based on Equation (23)).

No.	Model parameter	Mean brachial flow	Systolic radial pressure
8	Diameter tapering of innominate, subclavian, axillary, and brachial arteries	3	
15	Diameter tapering of the innominate, subclavian, axillary, and brachial arteries	10	2
16	Diameter of the radial artery		1
19	Aortic diameter		2
20	Diameter of the basilic, axillary, and subclavian veins	1	
49	Aortic characteristic impedance	2	16
57	Aortic Windkessel resistance	21	21
61	Radial artery Windkessel compliance		3
67	Intravenous pressure	3	
68	Eccentricity ratio of the basilic, axillary, and subclavian veins	42	14
73	Mean aortic flow	11	35

Corresponds to the expected reduction of the total variance if this parameter is fixed as a percentage of the total variance (i.e. 100% times the main Sobol index).

DOI: 10.1002/cnm

Table III. Rounded reference values (%) corresponding to the total Sobol index of important parameters (based on Equation (23)).

No.	Model parameter	Mean brachial flow	Systolic radial pressure
8	Diameter tapering of innominate, subclavian, axillary, and brachial arteries	4	
15	Diameter tapering of the innominate, subclavian, axillary, and brachial arteries	11	2
16	Diameter of the radial artery		1
19	Aortic diameter		2
20	Diameter of the basilic, axillary, and subclavian veins	2	
49	Aortic characteristic impedance	2	19
57	Aortic Windkessel resistance	20	22
61	Radial artery Windkessel compliance		2
67	Intravenous pressure	3	
68	Eccentricity ratio of the basilic, axillary, and subclavian veins	46	13
73	Mean aortic flow	12	34

Corresponds to percentage of the total variance left if all other parameters are fixed (i.e. 100% times the total Sobol index S_T).

5.2. *Sensitivity analysis of the pulse wave propagation model*

We investigated how well the obtained metamodels were able to reconstruct the actual model outputs. This is quantified using adjusted R^2-values (Equation (21)), which are given in Table IV. The metamodel constructed with the expansion coefficients obtained with the regression approach shows good agreement with the model output in the sparse grid points as indicated by the adjusted R^2-values that are close to 1. The projection approach is not able to do this. The adjusted R^2-values are significantly larger than 1 or become negative.

Table IV. The adjusted R^2-values for each metamodel calculated with Equation (21).

	Mean flow				Systolic pressure			
	gPCE-R		gPCE-P		gPCE-R		gPCE-P	
	$l=1$	$l=2$	$l=1$	$l=2$	$l=1$	$l=2$	$l=1$	$l=2$
$z=1$	0.98	0.99	$\ll 0$	$\ll 0$	0.98	0.99	$\ll 0$	$\ll 0$
$z=2$	1.00	1.00	$\gg 1$	$\ll 0$	1.00	1.00	$\gg 1$	$\ll 0$
$z=3$	1.00	1.00	$\gg 1$	$\gg 1$	1.00	1.00	$\gg 1$	$\gg 1$

The results for parameter fixing are shown in Figures 3 and 4, and the results for parameter prioritization are shown in Figures 5 and 6. Each figure consists of a tableau of six plots spread over three rows and two columns. Each row corresponds to a particular maximum polynomial order ($z = \{1, 2, 3\}$ from top to bottom), and each column corresponds to a particular gPCE approach for finding the expansion coefficients: the left column contains the regression (gPCE-R) results, and the right column contains the projection (gPCE-P) results. The open markers correspond to sparse grid level $l = 1$, and the closed markers correspond to sparse grid level $l = 2$. The markers corresponding to the same parameter are linked by a line that is furthermore annotated with the parameter number.

5.2.1. *Comparison to reference: parameter fixing.*

5.2.1.1. Mean flow. The results for mean flow are shown in Figure 3. The horizontal and vertical dotted lines indicate the threshold value T, and the diagonal dotted line represents the agreement

DOI: 10.1002/cnm

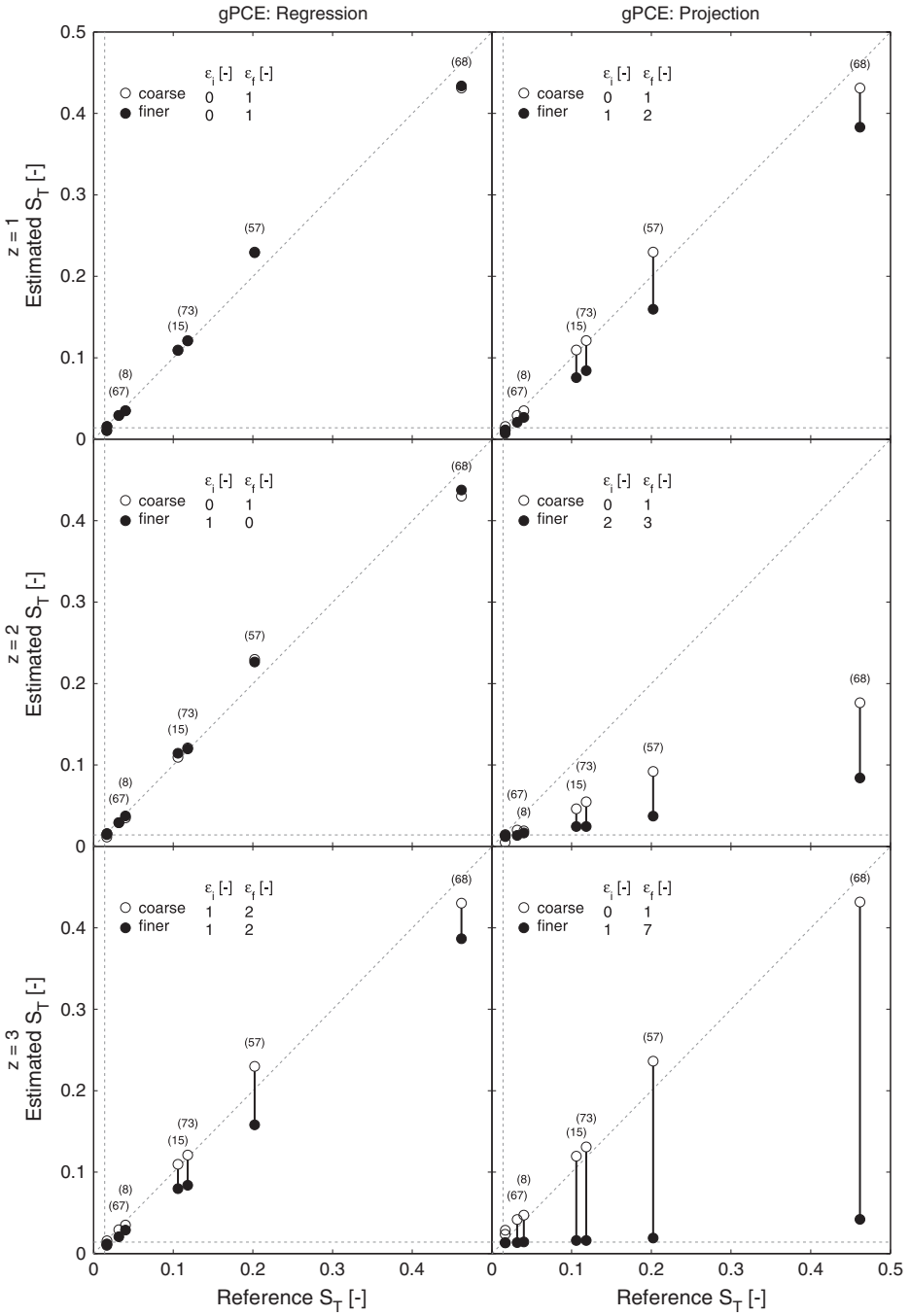

Figure 3. The estimated total sensitivity indices for the mean flow obtained using gPCE plotted against the reference total sensitivity indices S_T. Each row shows results obtained for a particular choice for the maximal polynomial order z. Each column shows results obtained either using the regression approach (first column) or using the projection approach (second column). The level of the sparse grid l is indicated by the color of the marker, with $l = 1$ corresponding to white and $l = 2$ corresponding to black. The number of parameters that are fixed based on gPCE but not based on the reference is given by ϵ_f, and the parameters that are not fixed based on gPCE but are fixed based on the reference are given by ϵ_i.

DOI: 10.1002/cnm

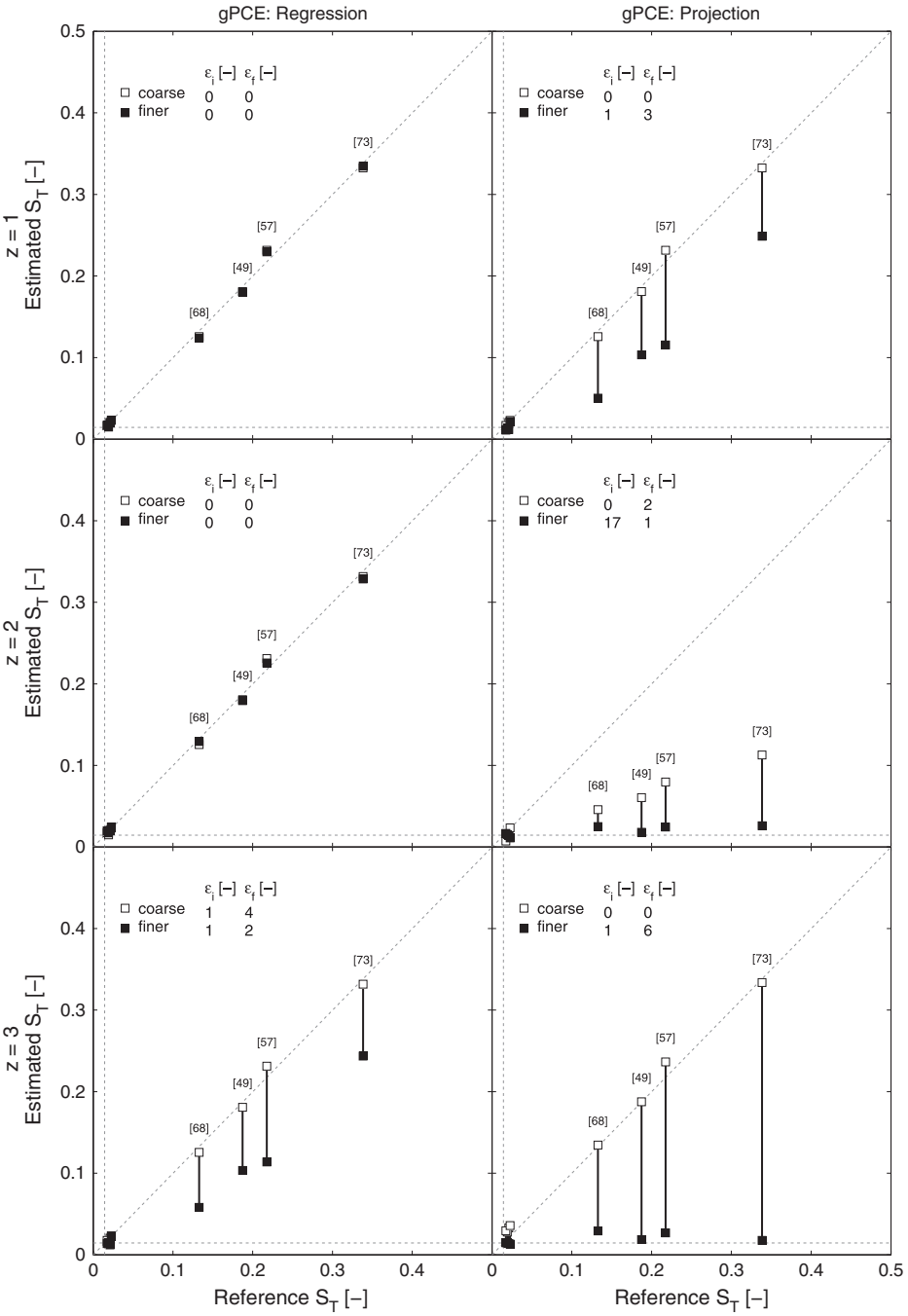

Figure 4. The estimated total sensitivity indices for the systolic pressure obtained using gPCE plotted against the reference total sensitivity indices S_T. Each row shows results obtained for a particular choice for the maximal polynomial order z. Each column shows results obtained either using the regression approach (first column) or using the projection approach (second column). The level of the sparse grid l is indicated by the color of the marker, with $l = 1$ corresponding to white and $l = 2$ corresponding to black. The number of parameters that are fixed based on gPCE but not based on the reference is given by ϵ_f, and the parameters that are not fixed based on gPCE but are fixed based on the reference are given by ϵ_i.

DOI: 10.1002/cnm

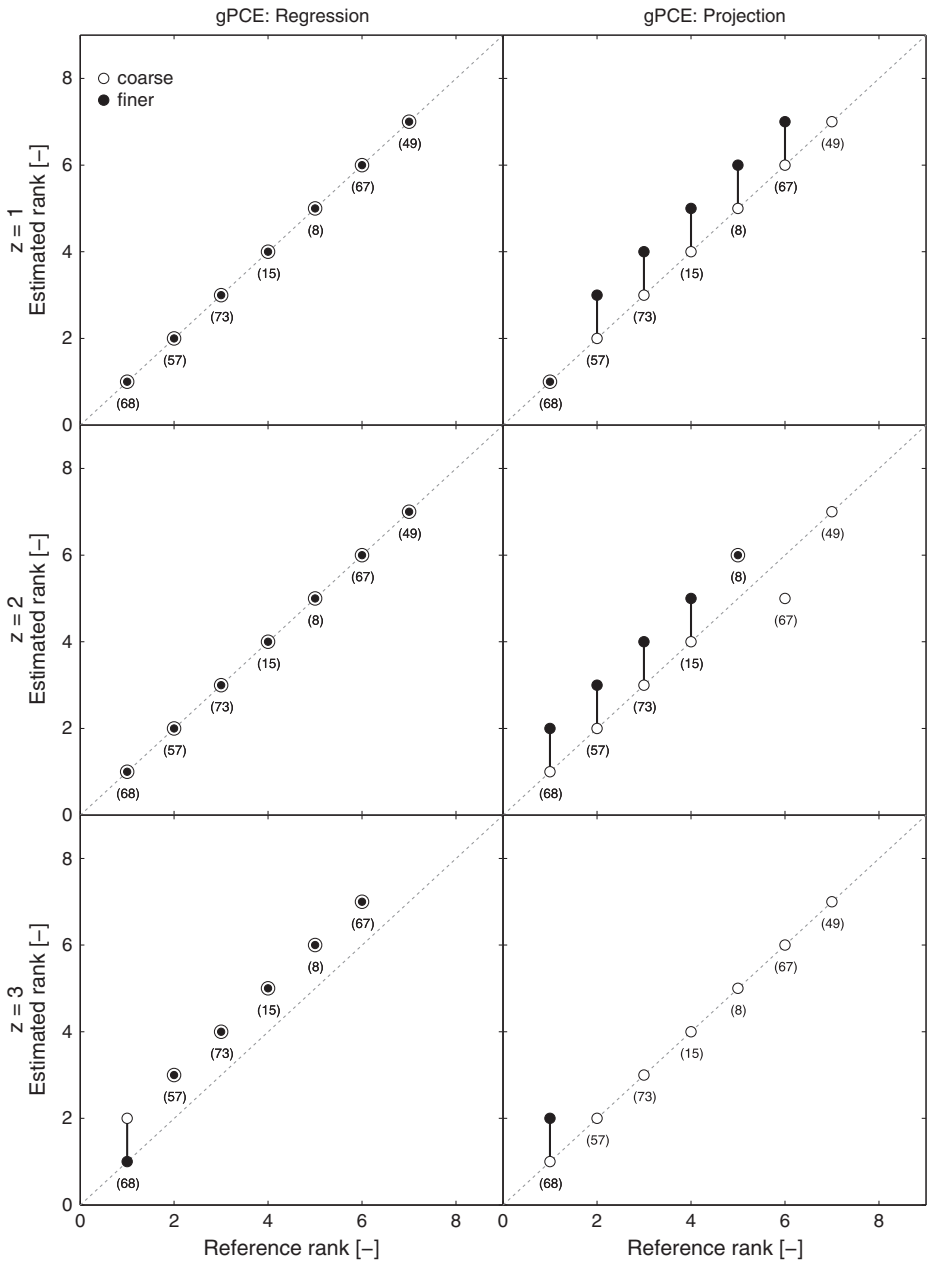

Figure 5. The estimated rank of the parameters identified as important for the mean flow. Each row shows results obtained for a particular choice for the maximal polynomial order z. Each column shows results obtained either using the regression approach (first column) or using the projection approach (second column). The level of the sparse grid l is indicated by the color of the marker, with $l = 1$ corresponding to white and $l = 2$ corresponding to black.

line. The number of parameters that are considered important by the gPCE method but not by the reference analysis is given by ϵ_{i}, and the number of parameters that are fixable according to the gPCE method but not fixable according to the reference is given by ϵ_{f}. For a linear metamodel ($z = 1$), the regression approach yields values for the total sensitivity indices that are close to the reference values using either a coarse ($l = 1$) or a fine ($l = 2$) sparse grid. Only one parameter is fixed according to the gPCE that is not fixed in the reference analysis ($\epsilon_{\mathrm{f}} = 1$) for both sparse grid levels. The projection approach does show differences in the total sensitivity indices obtained with different sparse grids: the coarse sparse grids yield better results than the fine sparse grid. This

DOI: 10.1002/cnm

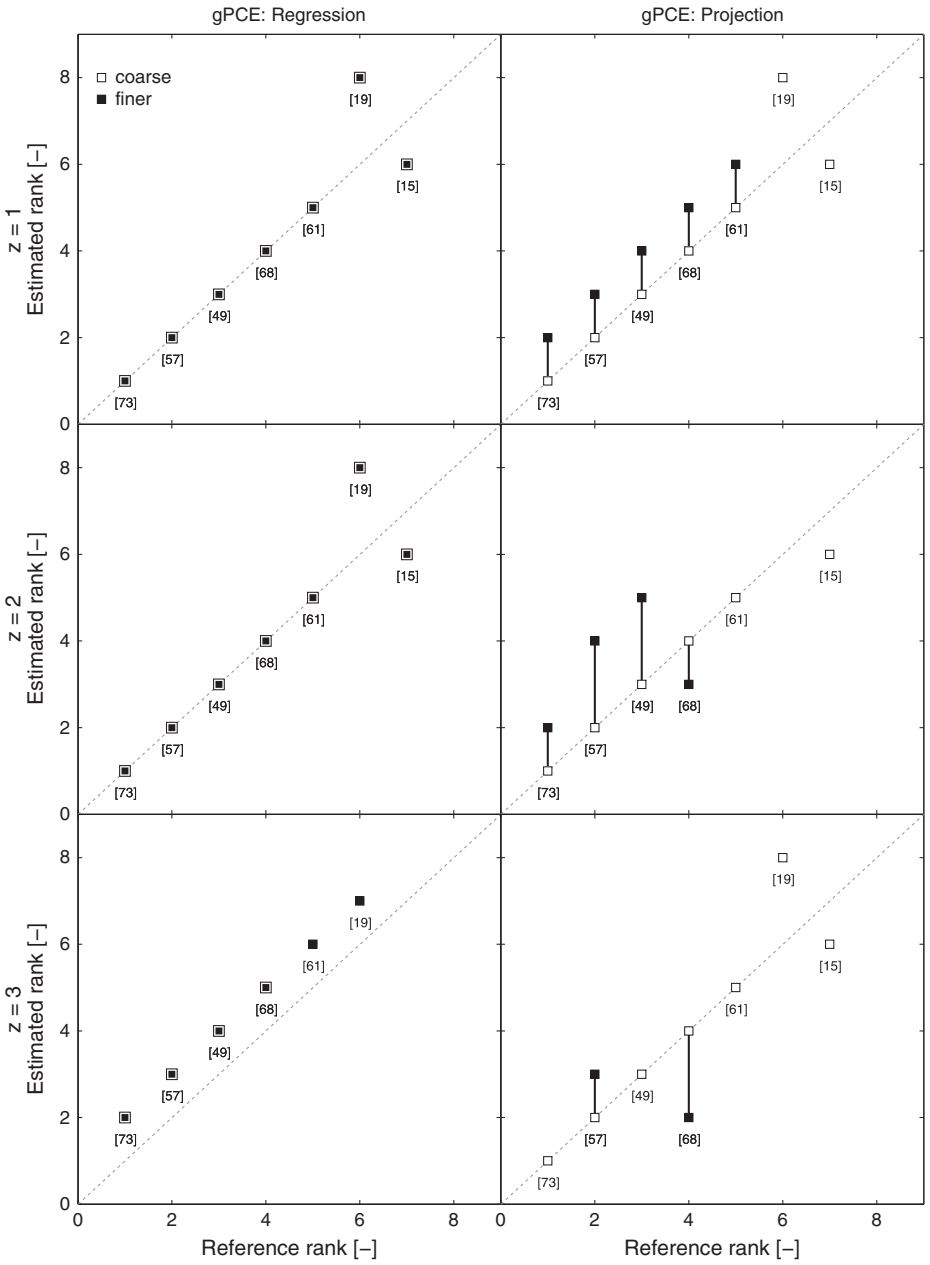

Figure 6. The estimated rank of the parameters identified as important for the systolic pressure. Each row shows results obtained for a particular choice for the maximal polynomial order z. Each column shows results obtained either using the regression approach (first column) or using the projection approach (second column). The level of the sparse grid l is indicated by the color of the marker, with $l = 1$ corresponding to light gray and $l = 2$ corresponding to dark gray.

is an unexpected result because a fine sparse grid has more samples and should provide a better approximation of the chaos coefficients. One parameter is fixed that is not fixed in the reference using the coarse grid ($\epsilon_f = 1$), whereas this is the case for two parameters in the fine sparse grid ($\epsilon_f = 2$).

For a quadratic metamodel ($z = 2$), the regression approach again yields good estimates of the total sensitivity indices for both sparse grids. Furthermore, the number of parameters that is unexpectedly fixed decreases from $\epsilon_f = 1$ to $\epsilon_f = 0$ by using a fine sparse grid. The projection approach yields bad estimates of the total sensitivity indices, the worst obtained using the fine sparse

DOI: 10.1002/cnm

grid. However, for the coarse grid, $\epsilon_f = 1$ and $\epsilon_f = 3$ for the fine grid, so the identified set of important parameters may still be acceptable.

For a third-order metamodel ($z = 3$), the regression approach shows different estimates of the total sensitivity indices for each sparse grid level. The better estimates are obtained with the coarse sparse grid, which again is unexpected. Both sparse grids result in $\epsilon_f = 2$. The projection approach yields better estimates of the total sensitivity indices for this metamodel than the quadratic metamodel when using a coarse sparse grid. The estimates obtained with a fine sparse grid deviate even more from the reference values. This is also reflected in the number of parameters that is fixed but that are not fixed in the reference, which increases from $\epsilon_f = 1$ (coarse grid) to $\epsilon_f = 7$ (fine grid).

5.2.1.2. Systolic pressure. Similar patterns to those described for the mean flow are observed when considering the systolic pressure as the output of interest. Therefore, the results in Figure 4 are not described in detail here.

5.2.2. Comparison to reference: parameter prioritization. According to the reference, there are eight important parameters for the mean flow and eight for the systolic pressure.

5.2.2.1. Mean flow. The results for the mean flow are shown in Figure 5. For a linear metamodel ($z = 1$), the regression approach yields seven out of eight important parameters. All are ranked correctly with respect to the reference. Increasing the sparse grid level does not change the ranking. The projection approach shows different results for different sparse grid levels. Seven important parameters are identified with the coarse grid. All seven are ranked in accordance with the reference. In the fine sparse grid, only one parameter is ranked similar to the reference. However, the remaining parameters have only moved one position in the ranking, and one parameter is no longer identified as important.

For a quadratic metamodel ($z = 2$), the regression approach yields seven out of eight important parameters with both the coarse and the fine grid. In both cases, the rankings are the same as the reference ranking. The projection approach identifies seven important parameters on the coarse grid, six of which are ranked the same as the reference. On the fine grid, only five important parameters are found, all of which have moved one spot up from the reference rankings.

For a third-order metamodel ($z = 3$), the regression approach yields six important parameters on both grids. On the coarse grid, all parameter rankings have moved one up from the reference rankings. The same is true for the fine grid, except for one parameter, which returns to its reference ranking. The projection approach yields seven important parameters on the coarse grid, all of which are ranked the same as in the reference. Only one important parameter is found on the coarse grid.

5.2.2.2. Systolic pressure. The results for the systolic pressure are shown in Figure 6. For a linear metamodel ($z = 1$), the regression method identifies seven parameters. All except two parameters are ranked in the same way as the reference. The results are not changed on the finer sparse grid. The projection approach gives similar results for the coarse grid. On the finer grid, the projection approach only yields five important parameters. All of these have a ranking that is one position off from the reference value.

For a quadratic metamodel ($z = 2$), the regression approach yields the same ranking as when using the linear metamodel. The projection yields six important parameters using the coarse sparse grid, five of which are ranked correctly with respect to the reference. Four important parameters are found using the fine sparse grid, but none are ranked in the same way as the reference. Parameters that were found on both sparse grids give worse results on the fine sparse grid.

For a third-order metamodel ($z = 3$), the regression approach yields four important parameters using the coarse sparse grid. All of these parameters have a rank that is one rank different from the reference rankings. Two additional important parameters are found when using the fine sparse grid, but the ranking is still one position off. When using the projection approach, seven important parameters are found using the coarse sparse grid, five of which are ranked correctly. On the fine grid, only two important parameters are found; the rankings of which do not correspond to the reference rankings.

DOI: 10.1002/cnm

6. DISCUSSION

Patient-specific cardiovascular modeling requires model personalization. More specifically, it is useful to know which model parameters are most rewarding to measure more accurately and in what order (parameter prioritization) and which parameters can be fixed (parameter fixing) so that you can optimize the measurement protocol. Variance-based global sensitivity analysis techniques yield sensitivity indices that can be used in these two settings.

Previously, a variance-based sensitivity analysis based on Saltelli's method was successfully applied to a pulse wave propagation model [42, 43]. It was shown that the model has the potential to support clinical decision-making for the creation of a vascular access for hemodialysis [51, 52]. Recently, a randomized multicenter clinical trial was initiated to assess the predictive value of this model.

Although Saltelli's method was successfully applied, its computational cost is relatively high. Therefore, the primary aim of this study was to apply the gPCE, which is generally less computationally expensive, to the previously developed pulse wave propagation model with 73 model parameters [22] and to examine whether this method results in the same conclusions with respect to model personalization as Saltelli's Monte Carlo method [30]. We analyzed the gPCE method by using both the spectral projection and the regression approaches for assessing the expansion coefficients of the gPCE. We considered the same outputs of interest as defined in our previous study where we applied Saltelli's method to this model [42]; that is, mean brachial artery flow and the systolic distal pressure in the radial artery at wrist level. The gPCE method generally requires significantly less model runs than Saltelli's method. However, in our case, the number of model parameters is so large that the use of the gPCE is only computationally rewarding when using sparse grid levels of $l \leqslant 2$, and therefore, we did not investigate for higher levels. However, we did perform full convergence analysis for several analytical functions (Appendix D) to ensure the correctness of our implementation. We found similar convergence behavior as already published in the literature [31]. As an alternative for the full convergence analysis of the pulse wave propagation model, we checked whether the obtained metamodels were able to reproduce the model output in the grid points. It was found that the regression approach was able to do this successfully, whereas the projection approach failed to obtain the model output accurately.

With respect to parameter fixing, we have found that the gPCE method for both outputs using the regression approach results in accurate estimates of the total sensitivity indices when the metamodel $z = \{1, 2\}$. For $z = 3$, the estimates become less accurate when a finer sparse grid is used. When we consider the set of parameters to be fixed, the regression approach identifies the same set as the reference in all cases except for the systolic pressure at $z = 3$ and a coarse grid. The gPCE method using the projection approach results in accurate estimates of the total sensitivity indices for $z = \{1, 3\}$ as long as a coarse grid is used. The estimates become worse when a finer sparse grid is used. The set of parameters that is fixed is similar to the reference set as long as a coarse sparse grid is used. When using a finer grid, less parameters are identified correctly as the metamodel order z increases.

With respect to parameter prioritization, the regression approach yields accurate results for $z = \{1, 2\}$, which slightly deteriorates for $z = 3$. When using a finer sparse grid, the results for $z = 3$ are slightly improved. The projection approach shows reasonably accurate results when using the coarse grid, despite the metamodel being unable to accurately reproduce the model output. For increasing metamodel order z, the obtained rankings become worse when using the finer sparse grid.

It must be kept in mind that the ranking obtained on the basis of the main sensitivity indices serves only as a guide for the priority in which the parameters should be measured more accurately. There may be practical limitations on the measurability of the obtained set of important parameters. Moreover, if two or more parameters have comparable main sensitivity indices, the exact order in which they are measured is not so important.

The results show that in general the projection approach does not perform as well as the regression approach. The difference can be attributed to the different ways in which the expansion coefficients are assessed. An integral is approximated by using the Smolyak algorithm when using spectral projection. Novak and Ritter [35] have shown that the error introduced by the Smolyak algorithm

DOI: 10.1002/cnm

depends on the number of model parameters, the smoothness of the model, and the grid level used. Furthermore, Crestaux *et al.* [31] found that, even for smooth functions, increasing the number of model parameters requires a higher Smolyak level. In our study, we used 73 model parameters, and it is therefore possible that we have not reached convergence yet.

To investigate this, a convergence analysis with respect to the level of the sparse grid is required. However, performing a complete convergence analysis for the pulse wave propagation model would require significant computational time as the number of model evaluations to estimate the expansion coefficients grow exponentially when the grid level increases. Alternative methods need to be developed that allow for a complete convergence analysis within acceptable computational time.

In addition to the compromising effect of the large number of model parameters on the Smolyak algorithm, the smoothness of the model is also not known *a priori*. It might be possible that the pulse wave propagation model is non-smooth, which hampers the accuracy of the integral approximation via the Smolyak algorithm. Non-smoothness in the output space might result from the relatively large uncertainty domains of the model input because of uncertainties of *in vivo* measurements in combination with the independent variation of these model parameters. Possible non-smoothness in the output space is not only affecting the integration during spectral projection but also the convergence of the gPCE itself, which is known as the Gibbs phenomenon [53, 54]. This phenomenon occurs when a discontinuity or a steep gradient in a piecewise smooth function is approximated by a global basis such as the Legendre polynomials used in gPCE. The expansion coefficients for the spectral projection approach are determined by integrating over the complete domain thus also across the discontinuities. This might result in less accurate estimates for the coefficients. Some work has been performed on detecting non-smoothness in multivariate space for stochastic simulations [55] that may help to circumvent this limitation. The reason that the lowest sparse grid level does not fail is then that the output space is not fully explored, thereby masking possible smoothness problems. The regression approach is less sensitive for non-smoothness as the expansion coefficients are assessed by least squares approximation and will only influence the regression approach when the number of points near the non-smoothness is large. However, be aware that the regression approach may suffer from overfitting or underfitting [31].

A limitation of the gPCE method is that the polynomial basis functions must be evaluated at each sample point. This is a preprocessing step that can become a significant portion of total computational time as the maximal polynomial order z increases (especially for models with many parameters and at high sparse grid levels). An alternative (but related) method that does not rely on a metamodel is based on Lagrangian interpolation of the output space [33]. This method has been applied for uncertainty quantification [32, 56] and for estimation of the main sensitivity index [57]. Although theory is available for estimating the total sensitivity indices using this method [58], we are not aware of its application in cardiovascular modeling. Unfortunately, the performance of the stochastic method based on construction of a Lagrangian interpolant is also sensitive to non-smoothness in the output space [53, 54].

Another limitation of this study is that both Saltelli's method and gPCE rely on the assumption of independent (uncorrelated) input parameters. Mathematical theory is actively being developed for variance-based sensitivity analysis for dependent (correlated) inputs; see, for example, Chastaing *et al.* [59], Mara *et al.* [60], and Zhou *et al.* [61]. Future work will consider these new approaches. However, a problem introduced with correlated input is that the correlations must be known, whereas these correlations are often not known in a clinical setting. Another limitation is that we assumed uniformly distributed inputs. Although other distributions can be used in each method discussed, these distributions must be parametrized based on large population studies or on repeated measurements in individuals. If any of the input distributions are known, they can be mixed in with the uniform distributions (i.e. the methods allow for different distributions for each parameter).

It is important to note that we checked whether the results were physically and physiologically plausible before performing the sensitivity analysis. This is mandatory because the large changes in input parameters could lead to changes in the mathematical behavior of the underlying partial differential equations; for example, from hyperbolic to parabolic [33].

For practical purposes, it might be beneficial to further reduce the computational cost of the presented sensitivity analysis by applying this quantitative sensitivity analysis methods only on a

DOI: 10.1002/cnm

subset consisting of important model parameters identified by the qualitative screening method of Morris [62]. This allows for convergence analysis at higher levels and will be the future work. Another possibility can be to use more efficient sampling strategies for the gPCE method using the regression approach, which are available in literature [34].

7. CONCLUSION

For model personalization of complex cardiovascular models, such as our pulse wave propagation model, the use of the polynomial chaos expansion may be an interesting alternative to the Saltelli method. However, be aware that the projection approach is hampered by a large number of parameters and possible non-smoothness, which affects the accuracy of the Smolyak algorithm. Therefore, it is recommended to use the regression approach. This approach yields good results as long as the maximal polynomial order of the metamodel does not allow for spurious high-order expansion terms. Saltelli's method is robuster for sensitivity and uncertainty analysis but requires (in general) much more model runs.

APPENDIX A: SOBOL DECOMPOSITION

The Sobol decomposition of a function f is as follows:

$$f(X_1,\ldots,X_k) = f_0 + \sum_{i=1}^{k} f_i(X_i) + \sum_{i=1}^{k}\sum_{j>i}^{k} f_{i,j}(X_i,X_j) + \ldots + f_{12\ldots k}(X_1,\ldots,X_k). \quad \text{(A.1)}$$

Herein, f_0 is a constant. When the integrals of all others summands over any of its parameters are zero, it can be shown that all summands are orthogonal and that the decomposition is unique [44]. Because of the uniqueness of the decomposition, each summand can be defined univocally. Indeed, each summand can be given by its conditional expected value. For example, the summands f_i and $f_{i,j}$ can be given by

$$f_i(X_i) = \int_{\Omega_{-i}} f(X_1,\ldots,X_k)\mathrm{d}\Omega_{-i} - f_0, \quad \text{(A.2)}$$

and

$$f_{i,j}(X_i,X_j) = \int_{\Omega_{-ij}} f(X_1,\ldots,X_k)\mathrm{d}\Omega_{-ij} - f_i(X_i) - f_j(X_j) - f_0, \quad \text{(A.3)}$$

respectively. Herein, Ω_{-i} indicates the domain Ω except the domain of X_i (i.e. Ω_i), while the integrals represent the conditional expected values given X_i ($\mathrm{E}(Y|X_i)$), and given X_i and X_j ($\mathrm{E}(Y|X_i,X_j)$), respectively. Note that f_0 equals the expected value of Y and that a uniform distribution on the domain Ω is assumed for the definition of the expected values. For the higher-order terms, similar equations as (A.2) and (A.3) can be derived.

APPENDIX B: COMPUTATIONAL COST ESTIMATION

In this appendix, an estimate for the number of required model runs to estimate the Sobol sensitivity indices is given when using crude Monte Carlo and Saltelli's efficient Monte Carlo approach.

The main Sobol sensitivity indices are given by $S_{i_1} = \mathrm{V}(\mathrm{E}(Y|X_{i_1}))/\mathrm{V}(Y)$, with $i_1 = 1,2,\ldots,k$. The total Sobol sensitivity indices are given by $S_{T_{i_1}} = \mathrm{E}(\mathrm{V}(Y|\mathbf{X}_{-i_1}))/\mathrm{V}(Y)$. Herein, E is the expected value, and V is the variance, which are expressed as multidimensional integrals.

B.1. Monte Carlo

For the estimation of the multidimensional integrals that define the Sobol main indices, we first need to calculate the expected value (sample mean) of Y given a fixed value of X_{i_1}. We need $N = \mathcal{O}(10^3)$

DOI: 10.1002/cnm

samples for this. To determine the variance of this expected value, integration over X_{i_1} is required. Thus, another $r = \mathcal{O}(10^3)$ samples for the value of X_{i_1} are needed. Therefore, the model must be evaluated for Nr samples in total. The sample variance is then taken from the corresponding Nr output samples. This is performed for all k parameters, resulting in Nrk model runs

To estimate the higher-order Sobol indices even more model runs are required [26].

B.2. Saltelli's method

Saltelli introduced a method that efficiently uses the available model evaluations. This method is based on two Latin hypercube sampled sets of $N = \mathcal{O}(10^3)$ parameter values; that is, $2N$ model runs. Another k additional sample sets are generated based on the original sampling sets by resampling all except one parameter; that is, $N(k+2)$ runs. Saltelli's method allows for the computation of all the main as well as the total sensitivity indices using only these samples. For details, we refer in [30].

APPENDIX C: SMOLYAK SPARSE GRID INTERPOLATION

First, consider the one-dimensional integral $\int_{x=-1}^{x=1} g(x)\mathrm{d}x$ on an arbitrary continuous function $g(x)$ defined on the domain $[-1, 1]$. When approximating this integral by using a one-dimensional quadrature formula of level $l = i - 1$ with $i \in \mathbb{N}$, the following general formulation can be derived:

$$\int_{x=-1}^{x=1} g(x)\mathrm{d}x \approx \sum_{j=1}^{m_i} g\left(x_j^i\right) \cdot w_j^i = U^i(g), \tag{C.1}$$

in which x_j^i is the jth integration point and w_j^i the nodal weight functions characterized by the demand that the approximation U^i is exact for all polynomials with an order less than $m_i \in \mathbb{N}$ and by the type of quadrature formula used. The weights and integration points used in this study will be explained later. The multidimensional integral in the numerator of Equation (18) can be approximated by the tensor products of the one-dimensional quadrature rules in each dimension; that is,

$$\int_\Omega Y(X_1, \ldots, X_k)\Psi_j(X_1, \ldots, X_k)\rho(X_1, \ldots, X_k)d\Omega = \int_\Omega G(X_1, \ldots, X_k)\mathrm{d}\Omega, \tag{C.2}$$

$$\approx \left(U^{i_1} \otimes \ldots \otimes U^{i_k}\right)(G) = \sum_{j_1=1}^{m_{i_1}} \ldots \sum_{j_k=1}^{m_{i_k}} G\left(X_{j_1^i}^{i_1}, \ldots, X_{j_k^i}^{i_k}\right) \cdot \left(w_{j_1^i}^{i_1} \cdot \ldots \cdot w_{j_k^i}^{i_k}\right). \tag{C.3}$$

The subscripts of the indices i and j denote the direction in which the one-dimensional quadrature formula is applied (e.g. k indicates in the direction of model parameter X_k). The formulation in (C.3) is called the tensor product algorithm (full tensorization). This algorithm requires a high number of support nodes $(m_{i_1}, \ldots, m_{i_k})$ sampled on the full grid. As a result, a large number of model evaluations are needed that will make this algorithm increasingly impractical when the number of model parameters increases. To reduce the number of support nodes, the Smolyak algorithm is used. The Smolyak algorithm maintains the approximation quality of the full tensorization up to logarithmic factor and is given by [35]

$$\int_\Omega G(X_1, \ldots, X_k)\mathrm{d}\Omega \approx \sum_{|\mathbf{i}| \leq q} \left(\Delta^{i_1} \otimes \ldots \otimes \Delta^{i_k}\right), \tag{C.4}$$

in which $\Delta^i = U^i - U^{i-1}$ for $i \in \mathbb{N}$ and $q \geqslant k$ is an integer defined as $l + k$. From here, we will refer to l as the Smolyak level. Moreover, $U^0 = 0$ and $|\mathbf{i}| = i_1 + \ldots + i_k$ is a multi-index for $\mathbf{i} \in \mathbb{N}^k$. It has been shown by Wasilkowski and Woźniakowski [37], and similar by Delvos [38], that Equation (C.4) can also be written as

$$\int_\Omega G(X_1, \ldots, X_k)\mathrm{d}\Omega \approx \sum_{l+1 \leqslant |\mathbf{i}| \leqslant q} (-1)^{q-|\mathbf{i}|} \cdot \binom{k-1}{q-|\mathbf{i}|} \cdot \left(U^{i_1} \otimes \ldots \otimes U^{i_k}\right)(G). \tag{C.5}$$

DOI: 10.1002/cnm

The tensor product algorithm $U^{i_1} \otimes \ldots \otimes U^{i_k}$ is based on the grid $X^{i_1} \times \ldots \times X^{i_k}$ in which $X^{i_k} = \{x_1^{i_1}, \ldots, x_k^{i_k}\} \subset [-1, 1]$ is the set of points corresponding to U^i in the kth direction. All grid points of the complete Smolyak algorithm are therefore given by

$$H(q,k) = \bigcup_{l+1 \leqslant |\mathbf{i}| \leqslant q} \left(X^{i_1} \times \ldots \times X^{i_k}\right). \tag{C.6}$$

When the nodal sets are nested, that is, $X^i \subset X^{i+1}$, then $H(q,k) \subset H(q+1,k)$ and the total number of grid points are reduced to

$$H(q,k) = \bigcup_{|\mathbf{i}|=q} \left(X^{i_1} \times \ldots \times X^{i_k}\right), \tag{C.7}$$

which is the most economical choice with respect to the number of model evaluations.

C.1. Clenshaw–Curtis grid points

The nodal points of the Clenshaw–Curtis method are the extrema of the Chebyshev polynomials, which are given by [35, 63]

$$x_j^i = -\cos\frac{\pi(j-1)}{m_i - 1} \qquad \text{with} \qquad j = 1, \ldots, m_i. \tag{C.8}$$

Because the number of points m_i in one dimension is odd, the weights functions of the Clenshaw–Curtis are defined by

$$w_1^i = w_{m_i}^i = \frac{1}{m_i(m_i-2)}, \tag{C.9}$$

for $j \in \{1, m_i\}$ and by

$$w_j^i = w_{m_i+1-j}^i = \frac{2}{m_i - 1}\left(1 - \frac{\cos(\pi(j-1))}{m_i(m_i-2)} - 2\sum_{s=1}^{(m_i-3)/2} \frac{1}{4s^2-1}\cos\frac{2\pi s(j-1)}{m_i-1}\right), \tag{C.10}$$

for $j = 2, \ldots, \frac{m_i-1}{2}$. Note that the set of j is reduced compared with the set in Equation (C.8) because of symmetry in the definition of the weight functions. Furthermore, m_1 is set to 1 to avoid that the number of points in the Smolyak algorithm increases too fast when the number of model parameters increases. Furthermore, x_1^1 is chosen to be 0 that results in $U^1(G) = 2G(0)$.

The number of sparse grid points (model evaluations) $n(q,k)$ can be expressed in the recursive formula given by Petras [64]

$$n(q+1, k+1) = \delta_0 n(q,k) + \sum_{\nu=1}^{l} \delta_\nu n(q-\nu, k), \tag{C.11}$$

$$\delta_\nu = \begin{cases} 1 & \text{if} \quad \nu = 0 \\ N(\nu,1) - N(\nu-1,1) & \text{else,} \end{cases} \tag{C.12}$$

$$n(q,1) = \begin{cases} 1 & \text{if} \quad q = 1 \\ 2^{q-1} + 1 & \text{else,} \end{cases} \tag{C.13}$$

when using the Clenshaw–Curtis integration method in one-dimensional. Note that δ_ν is the number of extra nodes of level ν with respect to the previous level in one-dimensional.

DOI: 10.1002/cnm

APPENDIX D: ANALYTICAL FUNCTIONS

We use the same analytical models in this study as used previously by Sudret *et al.* [34]. These models are selected for two specific reasons. First, the analytical models can serve as benchmark for the different uncertainty and sensitivity analysis methods because the sensitivity indices and output variances can be derived analytically. The second reason is that the mathematical behavior of these functions is known, which gives us the possibility to obtain more insights into the properties of the uncertainty and analysis tools used in this study.

D.1. Ishigami function

The first analytical model is the smooth, nonlinear, and monotonous Ishigami function defined as

$$Y = \sin X_1 + a \sin^2 X_2 + bX_3^4 \sin X_1, \tag{D.1}$$

with X_i is uniformly distributed over $[-\pi, \pi]$. The exact total and partial variances can be derived easily and are given by

$$\mathrm{V}(Y) = \frac{a^2}{8} + \frac{b\pi^4}{5} + \frac{b^2\pi^8}{18} + \frac{1}{2}, \tag{D.2}$$

$$\mathrm{V}(Y)|X_1) = \frac{b\pi^4}{5} + \frac{b^2\pi^8}{50} + \frac{1}{2},\ \mathrm{V}(Y|X_2) = \frac{a^2}{8},\ \mathrm{V}(Y|X_3) = 0, \tag{D.3}$$

$$\mathrm{V}(Y|X_1, X_2) = \mathrm{V}(Y|X_2, X_3) = \mathrm{V}(Y|X_1, X_2, X_3) = 0,\ \mathrm{V}(Y|X_1, X_3) = \frac{b^2\pi^8}{18} - \frac{b^2\pi^8}{50}. \tag{D.4}$$

In analogy to Sudret *et al.* [34], we have chosen $a = 7$ and $b = 0.1$.

D.2. Polynomial function

The second analytical model is a polynomial function given by

$$Y = \frac{1}{2^k} \prod_{i=1}^{k} \left(3X_i^2 + 1\right). \tag{D.5}$$

Herein are X_i the input variables ($i = 1, 2, \ldots, k$), uniformly distributed over the domain [0,1]. The sensitivity and total sensitivity indices are given analytically by

$$S_{i_1,\ldots,i_k} = \frac{5^{-s}}{(6/5)^k - 1}, \tag{D.6}$$

with $s = 1, \ldots, k$. Here, we set k to 3.

D.3. Sobol G-function

The third analytical function is the Sobol G-function. The Sobol G-function is a strongly non-monotonic, nonadditive function of k parameters X_i that are assumed to be identically and uniformly distributed over the domain [0, 1]. The Sobol G-function is defined as follows [28]:

$$G\left(X_1, \ldots, X_k, a_1, \ldots, a_k\right) = \prod_{i=1}^{k} g_i(X_i, a_i) \quad \text{with} \quad g_i(X_i, a_i) = \frac{|4X_i - 2| + a_i}{1 + a_i}. \tag{D.7}$$

For each of the $g_i(X_i, a_i)$ functions $\int_0^1 g_i(X_i, a_i)dx_i = 1$, and for $X_i \in [0, 1]$, the variation of the function is

$$1 - \frac{1}{1 + a_i} \leqslant g_i(X_i, a_i) \leqslant 1 + \frac{1}{1 + a_i}. \tag{D.8}$$

DOI: 10.1002/cnm

The main sensitivity indices can be obtained analytically from [28]

$$S_i = \frac{V_i}{V(Y)} = \frac{\mathrm{V}(\mathrm{E}(Y|X_i))}{\mathrm{V}(Y)} = \frac{1}{\mathrm{V}(Y)3(1+a_i)^2} \quad \text{with} \quad \mathrm{V}(Y) = \prod_{i=1}^{k}(1+V_i) - 1, \tag{D.9}$$

whereas the total sensitivity index is analytically expressed by [28]

$$S_{\mathrm{T},i} = \frac{\mathrm{E}(\mathrm{V}(Y|X_{-i}))}{\mathrm{V}(Y)} = \frac{V_i}{\mathrm{V}(Y)} \prod_{j \neq i}(1+V_j) \quad \text{with} \quad \mathrm{V}(Y) = \prod_{i=1}^{k}(1+V_i) - 1. \tag{D.10}$$

In this study, we consider eight input parameters and choose $X_5 = X_6 = X_7 = X_8 = \frac{1}{2}$ and $\mathbf{a} = [1, 2, 5, 10, 20, 50, 100, 500]$.

ACKNOWLEDGEMENTS

The authors acknowledge the European Commission 7th framework programme (ARCH ICT-224390) and (VPH-Share ICT-2009-6) for their funding.

Both authors contributed equally to the study.

REFERENCES

1. Sherwin SJ, Formaggia L, Peiró J. Computational modelling of 1D blood flow with variable mechanical properties and its application to the simulation of wave propagation in the human arterial system. *International Journal for Numerical Methods in Fluids* 2003; **43**:673–700.
2. Olufsen MS, Nadim A, Lipsitz La. Dynamics of cerebral blood flow regulation explained using a lumped parameter model. *American Journal of Physiology. Regulatory, Integrative and Comparative Physiology* 2002; **282**(2): R611–R622.
3. Liang F, Liu H. A closed-loop lumped parameter computational model for human cardiovascular system. *JSME International Journal Series C* 2005; **48**(4):484–493.
4. Westerhof N, Bosman F, de Vries CJ, Noordergraaf A. Analog studies of the human arterial tree. *Journal of Biomechanics* 1969; **2**:121–143.
5. Bessems D, Rutten MCM, van de Vosse FN. *Journal of Fluid Mechanics* 2007; **580**:145–168.
6. Stergiopulos N, Young DF, Rogge TR. Computer simulation of arterial flow with applications to arterial and aortic stenoses. *Journal of Biomechanics* 1992; **25**(12):1477–88.
7. Kharboutly Z, Fenech M, Treutenaere JM, Claude I, Legallais C. Investigations into the relationship between hemodynamics and vascular alterations in an established arteriovenous fistula. *Medical Engineering & Physics* 2007; **29**(9):999–1007.
8. Wenk JF, Papadopoulos P, Zohdi TI. Numerical modeling of stress in stenotic arteries with microcalcifications: a micromechanical approximation. *Journal of Biomechanical Engineering* 2010; **132**(9):1–11. DOI:10.1115/1.4001351.
9. van der Horst A, Boogaard FL, van't Veer M, Rutten MCM, Pijls NHJ, van de Vosse FN. Towards patient-specific modeling of coronary hemodynamics in healthy and diseased state. *Computational and Mathematical Methods in Medicine* 2013; **2013**:1–15. DOI:10.1155/2013/393792.
10. Wolters BJBM, Emmer M, Rutten MCM, Schurink GWH, van de Vosse FN. Assessment of endoleak significance after endovascular repair of abdominal aortic aneurysms: a lumped parameter model. *Medical Engineering & Physics* 2007; **29**(10):1106–1118.
11. Migliavacca F, Petrini L, Colombo M, Auricchio F, Pietrabissa R. Mechanical behavior of coronary stents investigated through the finite element method. *Journal of Biomechanics* June 2002; **35**(6):803–811.
12. Migliavacca F, Gervaso F, Prosi M, Zunino P, Minisini S, Formaggia L, Dubini G. Expansion and drug elution model of a coronary stent. *Computer Methods in Biomechanics and Biomedical Engineering* 2007; **10**(1):63–73.
13. Schampaert S, Rutten MCM, van T Veer M, van Nunen LX, Tonino PaL, Pijls NHJ, van de Vosse FN. Modeling the interaction between the intra-aortic balloon pump and the cardiovascular system: the effect of timing. *ASAIO Journal (American Society for Artificial Internal Organs : 1992)* 2013; **59**(1):30–36.
14. Alderliesten T, Konings MK, Niessen WJ. Simulation of minimally invasive vascular interventions for training purposes. *Computer Aided Surgery : Official Journal of the International Society for Computer Aided Surgery* 2004; **9**(1-2):3–15.
15. Euliano TY, Caton D, van Meurs W, Good ML. Modeling obstetric cardiovascular physiology on a full-scale patient simulator. *Journal of Clinical Monitoring* 1997; **13**(5):293–297.
16. van der Hout-van der Jagt MB, Oei SG, Bovendeerd PHM. A mathematical model for simulation of early decelerations in the cardiotocogram during labor. *Medical Engineering & Physics* 2012; **34**(5):579–89.

17. Leguy CAD, Bosboom EMH, Gelderblom H, Hoeks APG, van de Vosse FN. Estimation of distributed arterial mechanical properties using a wave propagation model in a reverse way. *Medical Engineering & Physics* 2010; **32**(9):957–67.
18. Stergiopulos N, Meister JJ, Westerhof N. Evaluation of methods for estimation of total arterial compliance. *The American Journal of Physiology* 1995; **268**(4 Pt 2):H1540–H1548.
19. Stergiopulos N, Westerhof BE, Westerhof N. Total arterial inertance as the fourth element of the Windkessel model. *The American Journal of Physiology* 1999; **276**(1 Pt 2):H81–H88.
20. Speelman L, Bosboom EMH, Schurink GWH, Hellenthal FAMVI, Buth J, Breeuwer M, Jacobs MJ, van de Vosse FN. Patient-specific AAA wall stress analysis: 99-percentile versus peak stress. *European Journal of Vascular and Endovascular Surgery : The Official Journal of the European Society for Vascular Surgery* 2008; **36**(6):668–676.
21. Pijls NHJ, van Gelder B, van der Voort P, Peels K, Bracke FALE, Bonnier HJRM, El Gamal MIH. Fractional flow reserve: a useful index to evaluate the influence of an epicardial coronary stenosis on myocardial blood flow. *Circulation* 1995; **92**:3183–3193.
22. Huberts W, Bode AS, Kroon W, Planken RN, Tordoir JHM, van de Vosse FN, Bosboom EMH. A pulse wave propagation model to support decision-making in vascular access planning in the clinic. *Medical Engineering & Physics* 2012; **34**(2):233–48.
23. Marchandise E, Willemet M, Lacroix V. A numerical hemodynamic tool for predictive vascular surgery. *Medical Engineering & Physics* 2009; **31**(1):131–144.
24. Hanna SR. Air quality model evaluation and uncertainty. *Journal of the Air Pollution Control Association* 1988; **38**(4):406–412.
25. USEPA. Guidance on the development, evaluation, and application of environmental models. *Technical Report*, United Sates Environmental Protection Agency, Council for Regulatory Environmental Modeling: Washington, DC (United States), 2009.
26. Saltelli A, Tarantola S, Campolongo F, Ratto M. *Sensitivity Analysis in Practice. A Guide to Assessing Scientific Models*. John Wiley & Sons, Ltd: Chichester, West Sussex (England), 2004.
27. Saltelli A, Ratto M, Anders T. *Global Sensitivity Analysis, the Primer*. John Wiley & Sons, Ltd: Chichester, West Sussex (England), 2008.
28. Saltelli A, Annoni P, Azzini I, Campolongo F, Ratto M, Tarantola S. Variance based sensitivity analysis of model output. Design and estimator for the total sensitivity index. *Computer Physics Communications* 2010; **181**(2): 259–270.
29. Homma T, Saltelli A. Importance measures in global sensitivity analysis of nonlinear models. *Reliability Engineering and System Safety* 1996; **52**:1–17.
30. Saltelli A. Making best use of model evaluations to compute sensitivity indices. *Computer Physics Communications* 2002; **145**(2):280–297.
31. Crestaux T, Le Maître O, Martinez JM. Polynomial chaos expansion for sensitivity analysis. *Reliability Engineering & System Safety* 2009; **94**(7):1161–1172.
32. Xiu D, Karniadakis GEM. The Wiener–Askey polynomial chaos for stochastic differential equations. *SIAM Journal on Scientific Computing* 2002; **24**(2):619–644.
33. Xiu D. Efficient collocational approach for parametric uncertainty analysis. *Communications in Computational Physics* 2007; **2**(2):293–309.
34. Sudret B. Global sensitivity analysis using polynomial chaos expansions. *Reliability Engineering & System Safety* 2008; **93**(7):964–979.
35. Novak E, Ritter K. High dimensional integration of smooth functions over cubes. *Numerische Mathematik* 1996; **75**:79–97.
36. Smolyak SA. Quadrature and interpolation formulas for tensor products of certain classes of functions. *Doklady Akademii Nauk SSSR* 1963; **4**:240–243.
37. Wasilkowski GW, Wozniakowski H. Explicit cost bounds multivariate tensor product problems. *Journal of Complexity* 1995; **11**:1–56.
38. Delvos FJ. D-variate Boolean interpolation. *Journal of Approximation Theory* 1982; **34**(2):99–114.
39. Wenk JF. Numerical modeling of stress in stenotic arteries with microcalcifications: a parameter sensitivity study. *Journal of Biomechanical Engineering* 2010; **133**(1):6.
40. Xiu D, Sherwin SJ. Parametric uncertainty analysis of pulse wave propagation in a model of a human arterial network. *Journal of Computational Physics* 2007; **226**(2):1385–1407.
41. Bode A, Caroli A, Huberts W, Planken N, Antiga L, Bosboom M, Remuzzi A, Tordoir J. Clinical study protocol for the ARCH project – computational modeling for improvement of outcome after vascular access creation. *The Journal of Vascular Access* 2011; **12**(4):369–76.
42. Huberts W, de Jonge C, van der Linden WPM, Inda MA, Tordoir JHM, Bosboom, van de Vosse FN, Bosboom EMH. A sensitivity analysis of a personalized pulse wave propagation model for arteriovenous fistula surgery. Part A: identification of most influential model parameters. *Medical Engineering and Physics* 2013; **35**(6):810–826.
43. Huberts W, de Jonge C, van der Linden WPM, Inda Ma, Passera K, Tordoir JHM, van de Vosse FN, Bosboom EMH. A sensitivity analysis of a personalized pulse wave propagation model for arteriovenous fistula surgery. Part B: identification of possible generic model parameters. *Medical Engineering & Physics* 2013; **35**(6):827–837.
44. Sobol I. Global sensitivity indices for nonlinear mathematical models and their Monte Carlo estimates. *Mathematics and Computers in Simulation* 2001; **55**:271–280.

DOI: 10.1002/cnm

45. Sudret B, Berveiller M, Lemaire M. A stochastic finite element procedure for moment and reliability analysis a stochastic finite element procedure for moment and reliability analysis. *European Journal of Computational Mechanics/Revue Européenne de Mécanique Numérique* 2006; **15**(7-6):825–866.
46. Hughes TJR, Lubliner J. On the one-dimensional theory of blood flow in the larger vessels. *Mathematical Biosciences* 1973; **18**:161–170.
47. Gardel A. Les pertes de charge dans les écoulements au travers de branchements en té. *Bulletin Technique de la Suisse Romande* 1957; **83**(9):123–130.
48. Gardel A. Les pertes de charge dans les écoulements au travers de branchements en té. *Bulletin Technique de la Suisse Romande* 1957; **83**(10):143–148.
49. Ohtmer O. Nonlinear flow analysis in pipe networks. *International Journal for Numerical Methods in Engineering* 1983; **19**:373–392.
50. Westerhof N, Lankhaar JW, Westerhof BE. The arterial Windkessel. *Medical & Biological Engineering & Computing* 2009; **47**(2):131–41.
51. Bode AS, Huberts W, Bosboom EMH, Kroon W, van der Linden WPM, Planken RN, van de Vosse FN, Tordoir JHM. Patient-specific computational modeling of upper extremity arteriovenous fistula creation: its feasibility to support clinical decision-making. *PLoS ONE* 2012; **7**(4):e34 491.
52. Caroli A, Manini S, Antiga L, Passera K, Ene-Iordache B, Rota S, Remuzzi G, Bode A, Leermakers J, van de Vosse FN, Vanholder R, Malovrh M, Tordoir J, Remuzzi A. Validation of a patient-specific hemodynamic computational model for surgical planning of vascular access in hemodialysis patients. *Kidney International* 2013; **84**(6):1237–45.
53. Gottlieb S, Jung JH, Kim S. A review of David Gottlieb's work on the resolution of the Gibbs phenomenon. *Communications in Computational Physics* 2011; **9**(3):497–519.
54. Xiu D. *Numerical Methods for Stochastic Computations – A Spectral Method Approach*. Princeton University Press: Princeton, New Jersey (United States), 2010.
55. Archibald R, Gelb A, Saxena R, Xiu D. Discontinuity detection in multivariate space for stochastic simulations. *Journal of Computational Physics* 2009; **228**(7):2676–2689.
56. Sankaran S, Marsden AL. A stochastic collocation method for uncertainty quantification and propagation in cardiovascular simulations. *Journal of Biomechanical Engineering* 2011; **133**(3):1–15. DOI:10.1155/2013/393792.
57. Chen P, Quarteroni A, Rozza G. Simulation-based uncertainty quantification of human arterial network hemodynamics. *International Journal for Numerical Methods in Biomedical Engineering* 2013; **29**:698–721.
58. Buzzard GT, Xiu D. Variance-based global sensitivity analysis via sparse-grid interpolation and cubature. *Communications in Computational Physics* 2011; **9**(3):542–567.
59. Chastaing G, Gamboa F, Prieur C. Generalized Hoeffding–Sobol decomposition for dependent variables – application to sensitivity analysis. *Electronic Journal of Statistics* 2012; **6**:2420–2448.
60. Mara TA, Tarantola S. Variance-based sensitivity indices for models with dependent inputs. *Reliability Engineering & System Safety* 2012; **107**:115–121.
61. Zhou C, Lu Z, Li G. A new algorithm for variance-based importance measures and importance kernel sensitivity. *Proceedings of the Institution of Mechanical Engineers, Part O: Journal of Risk and Reliability* 2012; **227**(1):16–27.
62. Morris MD. Factorial sampling plans for preliminary computational experiments. *Technometrics* 1991; **33**(2): 161–174.
63. Imhof JP. On the method for numerical integration of Clenshaw and Curtis. *Numerische Mathematik* 1963; **5**: 138–141.
64. Petras K. Smolyak cubature of given polynomial degree with few nodes for increasing dimension. *Numerische Mathematik* 2003; **93**:729–753.

DOI: 10.1002/cnm